Search for a *CP*-odd light Higgs boson in $J/\psi \to \gamma A^0$

M. Ablikim,[1] M. N. Achasov,[10,b] P. Adlarson,[68] S. Ahmed,[14] M. Albrecht,[4] R. Aliberti,[28] A. Amoroso,[67a,67c] M. R. An,[32] Q. An,[64,50] X. H. Bai,[58] Y. Bai,[49] O. Bakina,[29] R. Baldini Ferroli,[23a] I. Balossino,[24a] Y. Ban,[39,h] K. Begzsuren,[26] N. Berger,[28] M. Bertani,[23a] D. Bettoni,[24a] F. Bianchi,[67a,67c] J. Bloms,[61] A. Bortone,[67a,67c] I. Boyko,[29] R. A. Briere,[5] H. Cai,[69] X. Cai,[1,50] A. Calcaterra,[23a] G. F. Cao,[1,55] N. Cao,[1,55] S. A. Cetin,[54a] J. F. Chang,[1,50] W. L. Chang,[1,55] G. Chelkov,[29,a] D. Y. Chen,[6] G. Chen,[1] H. S. Chen,[1,55] M. L. Chen,[1,50] S. J. Chen,[35] X. R. Chen,[25] Y. B. Chen,[1,50] Z. J. Chen,[20,i] W. S. Cheng,[67c] G. Cibinetto,[24a] F. Cossio,[67c] X. F. Cui,[36] H. L. Dai,[1,50] X. C. Dai,[1,55] A. Dbeyssi,[14] R. E. de Boer,[4] D. Dedovich,[29] Z. Y. Deng,[1] A. Denig,[28] I. Denysenko,[29] M. Destefanis,[67a,67c] F. De Mori,[67a,67c] Y. Ding,[33] C. Dong,[36] J. Dong,[1,50] L. Y. Dong,[1,55] M. Y. Dong,[1,50,55] X. Dong,[69] S. X. Du,[72] Y. L. Fan,[69] J. Fang,[1,50] S. S. Fang,[1,55] Y. Fang,[1] R. Farinelli,[24a] L. Fava,[67b,67c] F. Feldbauer,[4] G. Felici,[23a] C. Q. Feng,[64,50] J. H. Feng,[51] M. Fritsch,[4] C. D. Fu,[1] Y. Gao,[64,50] Y. Gao,[39,h] Y. G. Gao,[6] I. Garzia,[24a,24b] P. T. Ge,[69] C. Geng,[51] E. M. Gersabeck,[59] A. Gilman,[62] K. Goetzen,[11] L. Gong,[33] W. X. Gong,[1,50] W. Gradl,[28] M. Greco,[67a,67c] L. M. Gu,[35] M. H. Gu,[1,50] C. Y. Guan,[1,55] A. Q. Guo,[25] A. Q. Guo,[22] L. B. Guo,[34] R. P. Guo,[41] Y. P. Guo,[9,f] A. Guskov,[29,a] T. T. Han,[42] W. Y. Han,[32] X. Q. Hao,[15] F. A. Harris,[57] K. L. He,[1,55] F. H. Heinsius,[4] C. H. Heinz,[28] Y. K. Heng,[1,50,55] C. Herold,[52] M. Himmelreich,[11,d] T. Holtmann,[4] G. Y. Hou,[1,55] Y. R. Hou,[55] Z. L. Hou,[1] H. M. Hu,[1,55] J. F. Hu,[48,j] T. Hu,[1,50,55] Y. Hu,[1] G. S. Huang,[64,50] L. Q. Huang,[65] X. T. Huang,[42] Y. P. Huang,[1] Z. Huang,[39,h] T. Hussain,[66] N. Hüsken,[22,28] W. Ikegami Andersson,[68] W. Imoehl,[22] M. Irshad,[64,50] S. Jaeger,[4] S. Janchiv,[26] Q. Ji,[1] Q. P. Ji,[15] X. B. Ji,[1,55] X. L. Ji,[1,50] Y. Y. Ji,[42] H. B. Jiang,[42] X. S. Jiang,[1,50,55] J. B. Jiao,[42] Z. Jiao,[18] S. Jin,[35] Y. Jin,[58] M. Q. Jing,[1,55] T. Johansson,[68] N. Kalantar-Nayestanaki,[56] X. S. Kang,[33] R. Kappert,[56] M. Kavatsyuk,[56] B. C. Ke,[44,1] I. K. Keshk,[4] A. Khoukaz,[61] P. Kiese,[28] R. Kiuchi,[1] R. Kliemt,[11] L. Koch,[30] O. B. Kolcu,[54a,m] B. Kopf,[4] M. Kuemmel,[4] M. Kuessner,[4] A. Kupsc,[37,68] M. G. Kurth,[1,55] W. Kühn,[30] J. J. Lane,[59] J. S. Lange,[30] P. Larin,[14] A. Lavania,[21] L. Lavezzi,[67a,67c] Z. H. Lei,[64,50] H. Leithoff,[28] M. Lellmann,[28] T. Lenz,[28] C. Li,[40] C. H. Li,[32] Cheng Li,[64,50] D. M. Li,[72] F. Li,[1,50] G. Li,[1] H. Li,[64,50] H. Li,[44] H. B. Li,[1,55] H. J. Li,[15] H. N. Li,[48,j] J. L. Li,[42] J. Q. Li,[4] J. S. Li,[51] Ke Li,[1] L. K. Li,[1] Lei Li,[3] P. R. Li,[31,k,l] S. Y. Li,[53] W. D. Li,[1,55] W. G. Li,[1] X. H. Li,[64,50] X. L. Li,[42] Xiaoyu Li,[1,55] Z. Y. Li,[51] H. Liang,[64,50] H. Liang,[1,55] H. Liang,[27] Y. F. Liang,[46] Y. T. Liang,[25] G. R. Liao,[12] L. Z. Liao,[1,55] J. Libby,[21] C. X. Lin,[51] D. X. Lin,[25] T. Lin,[1] B. J. Liu,[1] C. X. Liu,[1] D. Liu,[14,64] F. H. Liu,[45] Fang Liu,[1] Feng Liu,[6] G. M. Liu,[48,j] H. M. Liu,[1,55] Huanhuan Liu,[1] Huihui Liu,[16] J. B. Liu,[64,50] J. L. Liu,[65] J. Y. Liu,[1,55] K. Liu,[1] K. Y. Liu,[33] Ke Liu,[17,n] L. Liu,[64,50] M. H. Liu,[9,f] P. L. Liu,[1] Q. Liu,[55] Q. Liu,[69] S. B. Liu,[64,50] T. Liu,[1,55] W. M. Liu,[64,50] X. Liu,[31,k,l] Y. Liu,[31,k,l] Y. B. Liu,[36] Z. A. Liu,[1,50,55] Z. Q. Liu,[42] X. C. Lou,[1,50,55] F. X. Lu,[51] H. J. Lu,[18] J. D. Lu,[1,55] J. G. Lu,[1,50] X. L. Lu,[1] Y. Lu,[1] Y. P. Lu,[1,50] C. L. Luo,[34] M. X. Luo,[71] P. W. Luo,[51] T. Luo,[9,f] X. L. Luo,[1,50] X. R. Lyu,[55] F. C. Ma,[33] H. L. Ma,[1] L. L. Ma,[42] M. M. Ma,[1,55] Q. M. Ma,[1] R. Q. Ma,[1,55] R. T. Ma,[55] X. X. Ma,[1,55] X. Y. Ma,[1,50] F. E. Maas,[14] M. Maggiora,[67a,67c] S. Maldaner,[4] S. Malde,[62] Q. A. Malik,[66] A. Mangoni,[23b] Y. J. Mao,[39,h] Z. P. Mao,[1] S. Marcello,[67a,67c] Z. X. Meng,[58] J. G. Messchendorp,[56] G. Mezzadri,[24a] T. J. Min,[35] R. E. Mitchell,[22] X. H. Mo,[1,50,55] N. Yu. Muchnoi,[10,b] H. Muramatsu,[60] S. Nakhoul,[11,d] Y. Nefedov,[29] F. Nerling,[11,d] I. B. Nikolaev,[10,b] Z. Ning,[1,50] S. Nisar,[8,g] S. L. Olsen,[55] Q. Ouyang,[1,50,55] S. Pacetti,[23b,23c] X. Pan,[9,f] Y. Pan,[59] A. Pathak,[1] A. Pathak,[27] P. Patteri,[23a] M. Pelizaeus,[4] H. P. Peng,[64,50] K. Peters,[11,d] J. Pettersson,[68] J. L. Ping,[34] R. G. Ping,[1,55] S. Pogodin,[29] R. Poling,[60] V. Prasad,[64,50] H. Qi,[64,50] H. R. Qi,[53] M. Qi,[35] T. Y. Qi,[9] S. Qian,[1,50] W. B. Qian,[55] Z. Qian,[51] C. F. Qiao,[55] J. J. Qin,[65] L. Q. Qin,[12] X. P. Qin,[9] X. S. Qin,[42] Z. H. Qin,[1,50] J. F. Qiu,[1] S. Q. Qu,[36] K. H. Rashid,[66] K. Ravindran,[21] C. F. Redmer,[28] A. Rivetti,[67c] V. Rodin,[56] M. Rolo,[67c] G. Rong,[1,55] Ch. Rosner,[14] M. Rump,[61] H. S. Sang,[64] A. Sarantsev,[29,c] Y. Schelhaas,[28] C. Schnier,[4] K. Schoenning,[68] M. Scodeggio,[24a,24b] W. Shan,[19] X. Y. Shan,[64,50] J. F. Shangguan,[47] M. Shao,[64,50] C. P. Shen,[9] H. F. Shen,[1,55] X. Y. Shen,[1,55] H. C. Shi,[64,50] R. S. Shi,[1,55] X. Shi,[1,50] X. D. Shi,[64,50] J. J. Song,[15] J. J. Song,[42] W. M. Song,[27,1] Y. X. Song,[39,h] S. Sosio,[67a,67c] S. Spataro,[67a,67c] K. X. Su,[69] P. P. Su,[47] F. F. Sui,[42] G. X. Sun,[1] H. K. Sun,[1] J. F. Sun,[15] L. Sun,[69] S. S. Sun,[1,55] T. Sun,[1,55] W. Y. Sun,[27] X. Sun,[20,i] Y. J. Sun,[64,50] Y. Z. Sun,[1] Z. T. Sun,[1] Y. H. Tan,[69] Y. X. Tan,[64,50] C. J. Tang,[46] G. Y. Tang,[1] J. Tang,[51] J. X. Teng,[64,50] V. Thoren,[68] W. H. Tian,[44] Y. T. Tian,[25] I. Uman,[54b] B. Wang,[1] C. W. Wang,[35] D. Y. Wang,[39,h] H. J. Wang,[31,k,l] H. P. Wang,[1,55] K. Wang,[1,50] L. L. Wang,[1] M. Wang,[42] M. Z. Wang,[39,h] Meng Wang,[1,55] S. Wang,[9,f] W. Wang,[51] W. H. Wang,[69] W. P. Wang,[64,50] X. Wang,[39,h] X. F. Wang,[31,k,l] X. L. Wang,[9,f] Y. Wang,[51] Y. D. Wang,[38] Y. F. Wang,[1,50,55] Y. Q. Wang,[1] Y. Y. Wang,[31,k,l] Z. Wang,[1,50] Z. Y. Wang,[1] Ziyi Wang,[55] Zongyuan Wang,[1,55] D. H. Wei,[12] F. Weidner,[61] S. P. Wen,[1] D. J. White,[59] U. Wiedner,[4] G. Wilkinson,[62] M. Wolke,[68] L. Wollenberg,[4] J. F. Wu,[1,55] L. H. Wu,[1] L. J. Wu,[1,55] X. Wu,[9,f] X. H. Wu,[27] Z. Wu,[1,50] L. Xia,[64,50] H. Xiao,[9,f] S. Y. Xiao,[1] Z. J. Xiao,[34] X. H. Xie,[39,h] Y. G. Xie,[1,50] Y. H. Xie,[6] T. Y. Xing,[1,55] C. J. Xu,[51] G. F. Xu,[1] Q. J. Xu,[13] W. Xu,[1,55] X. P. Xu,[47] Y. C. Xu,[55] F. Yan,[9,f] L. Yan,[9,f] W. B. Yan,[64,50] W. C. Yan,[72] H. J. Yang,[43,e] H. X. Yang,[1] L. Yang,[44] S. L. Yang,[55] Y. X. Yang,[12] Yifan Yang,[1,55] Zhi Yang,[25] M. Ye,[1,50] M. H. Ye,[7] J. H. Yin,[1] Z. Y. You,[51] B. X. Yu,[1,50,55] C. X. Yu,[36]

G. Yu,[1,55] J. S. Yu,[20,i] T. Yu,[65] C. Z. Yuan,[1,55] L. Yuan,[2] X. Q. Yuan,[39,h] Y. Yuan,[1] Z. Y. Yuan,[51] C. X. Yue,[32] A. A. Zafar,[66] X. Zeng Zeng,[6] Y. Zeng,[20,i] A. Q. Zhang,[1] B. X. Zhang,[1] Guangyi Zhang,[15] H. Zhang,[64] H. H. Zhang,[51] H. H. Zhang,[27] H. Y. Zhang,[1,50] J. J. Zhang,[44] J. L. Zhang,[70] J. Q. Zhang,[34] J. W. Zhang,[1,50,55] J. Y. Zhang,[1] J. Z. Zhang,[1,55] Jianyu Zhang,[1,55] Jiawei Zhang,[1,55] L. M. Zhang,[53] L. Q. Zhang,[51] Lei Zhang,[35] S. Zhang,[51] S. F. Zhang,[35] Shulei Zhang,[20,i] X. D. Zhang,[38] X. Y. Zhang,[42] Y. Zhang,[62] Y. T. Zhang,[72] Y. H. Zhang,[1,50] Yan Zhang,[64,50] Yao Zhang,[1] Z. Y. Zhang,[69] G. Zhao,[1] J. Zhao,[32] J. Y. Zhao,[1,55] J. Z. Zhao,[1,50] Lei Zhao,[64,50] Ling Zhao,[1] M. G. Zhao,[36] Q. Zhao,[1] S. J. Zhao,[72] Y. B. Zhao,[1,50] Y. X. Zhao,[25] Z. G. Zhao,[64,50] A. Zhemchugov,[29,a] B. Zheng,[65] J. P. Zheng,[1,50] Y. H. Zheng,[55] B. Zhong,[34] C. Zhong,[65] L. P. Zhou,[1,55] Q. Zhou,[1,55] X. Zhou,[69] X. K. Zhou,[55] X. R. Zhou,[64,50] X. Y. Zhou,[32] A. N. Zhu,[1,55] J. Zhu,[36] K. Zhu,[1] K. J. Zhu,[1,50,55] S. H. Zhu,[63] T. J. Zhu,[70] W. J. Zhu,[36] W. J. Zhu,[9,f] Y. C. Zhu,[64,50] Z. A. Zhu,[1,55] B. S. Zou,[1] and J. H. Zou[1]

(BESIII Collaboration)

[1]*Institute of High Energy Physics, Beijing 100049, People's Republic of China*
[2]*Beihang University, Beijing 100191, People's Republic of China*
[3]*Beijing Institute of Petrochemical Technology, Beijing 102617, People's Republic of China*
[4]*Bochum Ruhr-University, D-44780 Bochum, Germany*
[5]*Carnegie Mellon University, Pittsburgh, Pennsylvania 15213, USA*
[6]*Central China Normal University, Wuhan 430079, People's Republic of China*
[7]*China Center of Advanced Science and Technology, Beijing 100190, People's Republic of China*
[8]*COMSATS University Islamabad, Lahore Campus, Defence Road, Off Raiwind Road, 54000 Lahore, Pakistan*
[9]*Fudan University, Shanghai 200443, People's Republic of China*
[10]*G.I. Budker Institute of Nuclear Physics SB RAS (BINP), Novosibirsk 630090, Russia*
[11]*GSI Helmholtzcentre for Heavy Ion Research GmbH, D-64291 Darmstadt, Germany*
[12]*Guangxi Normal University, Guilin 541004, People's Republic of China*
[13]*Hangzhou Normal University, Hangzhou 310036, People's Republic of China*
[14]*Helmholtz Institute Mainz, Staudinger Weg 18, D-55099 Mainz, Germany*
[15]*Henan Normal University, Xinxiang 453007, People's Republic of China*
[16]*Henan University of Science and Technology, Luoyang 471003, People's Republic of China*
[17]*Henan University of Technology, Zhengzhou 450001, People's Republic of China*
[18]*Huangshan College, Huangshan 245000, People's Republic of China*
[19]*Hunan Normal University, Changsha 410081, People's Republic of China*
[20]*Hunan University, Changsha 410082, People's Republic of China*
[21]*Indian Institute of Technology Madras, Chennai 600036, India*
[22]*Indiana University, Bloomington, Indiana 47405, USA*
[23a]*INFN Laboratori Nazionali di Frascati, I-00044 Frascati, Italy*
[23b]*INFN Sezione di Perugia, I-06100 Perugia, Italy*
[23c]*University of Perugia, I-06100 Perugia, Italy*
[24a]*INFN Sezione di Ferrara, I-44122 Ferrara, Italy*
[24b]*University of Ferrara, I-44122 Ferrara, Italy*
[25]*Institute of Modern Physics, Lanzhou 730000, People's Republic of China*
[26]*Institute of Physics and Technology, Peace Ave. 54B, Ulaanbaatar 13330, Mongolia*
[27]*Jilin University, Changchun 130012, People's Republic of China*
[28]*Johannes Gutenberg University of Mainz, Johann-Joachim-Becher-Weg 45, D-55099 Mainz, Germany*
[29]*Joint Institute for Nuclear Research, 141980 Dubna, Moscow region, Russia*
[30]*Justus-Liebig-Universitaet Giessen, II. Physikalisches Institut, Heinrich-Buff-Ring 16, D-35392 Giessen, Germany*
[31]*Lanzhou University, Lanzhou 730000, People's Republic of China*
[32]*Liaoning Normal University, Dalian 116029, People's Republic of China*
[33]*Liaoning University, Shenyang 110036, People's Republic of China*
[34]*Nanjing Normal University, Nanjing 210023, People's Republic of China*
[35]*Nanjing University, Nanjing 210093, People's Republic of China*
[36]*Nankai University, Tianjin 300071, People's Republic of China*
[37]*National Centre for Nuclear Research, Warsaw 02-093, Poland*
[38]*North China Electric Power University, Beijing 102206, People's Republic of China*
[39]*Peking University, Beijing 100871, People's Republic of China*
[40]*Qufu Normal University, Qufu 273165, People's Republic of China*
[41]*Shandong Normal University, Jinan 250014, People's Republic of China*

[42]*Shandong University, Jinan 250100, People's Republic of China*
[43]*Shanghai Jiao Tong University, Shanghai 200240, People's Republic of China*
[44]*Shanxi Normal University, Linfen 041004, People's Republic of China*
[45]*Shanxi University, Taiyuan 030006, People's Republic of China*
[46]*Sichuan University, Chengdu 610064, People's Republic of China*
[47]*Soochow University, Suzhou 215006, People's Republic of China*
[48]*South China Normal University, Guangzhou 510006, People's Republic of China*
[49]*Southeast University, Nanjing 211100, People's Republic of China*
[50]*State Key Laboratory of Particle Detection and Electronics, Beijing 100049, Hefei 230026, People's Republic of China*
[51]*Sun Yat-Sen University, Guangzhou 510275, People's Republic of China*
[52]*Suranaree University of Technology, University Avenue 111, Nakhon Ratchasima 30000, Thailand*
[53]*Tsinghua University, Beijing 100084, People's Republic of China*
[54a]*Turkish Accelerator Center Particle Factory Group, Istanbul Bilgi University, HEP Res. Cent., 34060 Eyup, Istanbul, Turkey*
[54b]*Near East University, Nicosia, North Cyprus, Mersin 10, Turkey*
[55]*University of Chinese Academy of Sciences, Beijing 100049, People's Republic of China*
[56]*University of Groningen, NL-9747 AA Groningen, Netherlands*
[57]*University of Hawaii, Honolulu, Hawaii 96822, USA*
[58]*University of Jinan, Jinan 250022, People's Republic of China*
[59]*University of Manchester, Oxford Road, Manchester, M13 9PL, United Kingdom*
[60]*University of Minnesota, Minneapolis, Minnesota 55455, USA*
[61]*University of Muenster, Wilhelm-Klemm-Strasse 9, 48149 Muenster, Germany*
[62]*University of Oxford, Keble Rd, Oxford, United Kingdom OX13RH*
[63]*University of Science and Technology Liaoning, Anshan 114051, People's Republic of China*
[64]*University of Science and Technology of China, Hefei 230026, People's Republic of China*
[65]*University of South China, Hengyang 421001, People's Republic of China*
[66]*University of the Punjab, Lahore-54590, Pakistan*
[67a]*University of Turin, I-10125 Turin, Italy*
[67b]*University of Eastern Piedmont, I-15121 Alessandria, Italy*
[67c]*INFN, I-10125 Turin, Italy*
[68]*Uppsala University, Box 516, SE-75120 Uppsala, Sweden*
[69]*Wuhan University, Wuhan 430072, People's Republic of China*
[70]*Xinyang Normal University, Xinyang 464000, People's Republic of China*
[71]*Zhejiang University, Hangzhou 310027, People's Republic of China*
[72]*Zhengzhou University, Zhengzhou 450001, People's Republic of China*

(Received 27 September 2021; accepted 7 January 2022; published 21 January 2022)

[a]Also at the Moscow Institute of Physics and Technology, Moscow 141700, Russia.
[b]Also at the Novosibirsk State University, Novosibirsk, 630090, Russia.
[c]Also at the NRC "Kurchatov Institute", PNPI, 188300, Gatchina, Russia.
[d]Also at Goethe University Frankfurt, 60323 Frankfurt am Main, Germany.
[e]Also at Key Laboratory for Particle Physics, Astrophysics and Cosmology, Ministry of Education; Shanghai Key Laboratory for Particle Physics and Cosmology; Institute of Nuclear and Particle Physics, Shanghai 200240, People's Republic of China.
[f]Also at Key Laboratory of Nuclear Physics and Ion-beam Application (MOE) and Institute of Modern Physics, Fudan University, Shanghai 200443, People's Republic of China.
[g]Also at Harvard University, Department of Physics, Cambridge, Massachusetts 02138, USA.
[h]Also at State Key Laboratory of Nuclear Physics and Technology, Peking University, Beijing 100871, People's Republic of China.
[i]Also at School of Physics and Electronics, Hunan University, Changsha 410082, China.
[j]Also at Guangdong Provincial Key Laboratory of Nuclear Science, Institute of Quantum Matter, South China Normal University, Guangzhou 510006, China.
[k]Also at Frontiers Science Center for Rare Isotopes, Lanzhou University, Lanzhou 730000, People's Republic of China.
[l]Also at Lanzhou Center for Theoretical Physics, Lanzhou University, Lanzhou 730000, People's Republic of China.
[m]Currently at Istinye University, 34010 Istanbul, Turkey.
[n]Henan University of Technology, Zhengzhou 450001, People's Republic of China.

Using J/ψ radiative decays from 9.0 billion J/ψ events collected by the BESIII detector, we search for di-muon decays of a CP-odd light Higgs boson (A^0), predicted by many new physics models beyond the Standard Model, including the next-to-minimal supersymmetric Standard Model. No evidence for the CP-odd light Higgs production is found, and we set 90% confidence level upper limits on the product branching fraction $\mathcal{B}(J/\psi \to \gamma A^0) \times \mathcal{B}(A^0 \to \mu^+\mu^-)$ in the range of $(1.2 - 778.0) \times 10^{-9}$ for $0.212 \le m_{A^0} \le 3.0$ GeV/c^2. The new measurement is a 6–7 times improvement over our previous measurement, and is also slightly better than the *BABAR* measurement in the low-mass region for $\tan\beta = 1$.

DOI: 10.1103/PhysRevD.105.012008

I. INTRODUCTION

The origin of mass is one of the most important questions in physics. The masses of the fundamental particles are generated through spontaneous breaking of electroweak symmetry by the Higgs mechanism [1]. The Higgs mechanism implies the existence of at least one new scalar particle, the Higgs boson, which was the last missing Standard Model (SM) particle. It was discovered by the Large Hadron Collider experiments at CERN [2] in July 2012 and has a profound effect on our fundamental understanding of matter.

Many models beyond the SM, such as the next-to-minimal supersymmetric Standard Model (NMSSM) [3–5], extend the Higgs sector to include additional Higgs fields. The NMSSM adds an additional singlet chiral superfield to the Minimal Supersymmetric Standard Model (MSSM) [6] to alleviate the so-called "little hierarchy problem" [7]. It contains three CP-even, two CP-odd, and two charged Higgs bosons [3,4]. The mass of the lightest Higgs boson, A^0, may be smaller than twice the mass of the charmed quark, thus making it accessible via $J/\psi \to \gamma A^0$ [8].

The branching fraction of $V \to \gamma A^0$ ($V = \Upsilon, J/\psi$) is expressed as [8–10]

$$\frac{\mathcal{B}(V \to \gamma A^0)}{\mathcal{B}(V \to l^+l^-)} = \frac{G_F m_q^2 g_q^2 C_{\rm QCD}}{\sqrt{2}\pi\alpha}\left(1 - \frac{m_{A^0}^2}{m_V^2}\right), \qquad (1)$$

where α is the fine structure constant, G_F is the Fermi coupling constant, $l \equiv e$ or μ, m_q is the quark mass, $C_{\rm QCD}$ includes the leptonic width of $\mathcal{B}(V \to l^+l^-)$ [11,12] as well as m_{A^0} dependent QCD and relativistic corrections to $\mathcal{B}(V \to \gamma A^0)$ [10], and g_q is the effective Yukawa coupling to the Higgs field to the up- or down-type quark-pair. In the NMSSM, $g_c = \cos\theta_A/\tan\beta$ ($q = c$) for the charm quark and $g_b = \cos\theta_A \tan\beta$ ($q = b$) for the bottom quark, where $\tan\beta$ is the ratio of up- and down-type Higgs doublets, and $\cos\theta_A$ is the fraction of the nonsinglet component of the A^0 [13,14]. The value of $\cos\theta_A$ is zero for a pure A^0 singlet state [15]. The branching fraction of $J/\psi \to \gamma A^0$ is predicted to be in the range of 10^{-9}–10^{-7} depending upon the A^0 mass and the NMSSM parameters [4]. The branching fraction of $A^0 \to \mu^+\mu^-$ is predicted to be much larger for $\tan\beta \ge 1$ [13]. An experimental study of such a low-mass Higgs boson is desirable to test the SM [16] and to look for new physics beyond the SM [3,4,17].

The *BABAR* [18], CLEO [19], and CMS [20] experiment have searched for dimuon decays of A^0, and placed a strong exclusion upper limit on g_b. On the other hand, the BESIII measurements, sensitive on g_c, is complementary to those by considering g_b. The recent BESIII measurement [21], based on 225 million J/ψ events, is slightly lower than the *BABAR* measurement [18] in the low-mass region for $\tan\beta \le 0.6$. The combined measurements of the BESIII and *BABAR* have revealed that the A^0 is mostly singlet in nature because of obtained upper limit on $\cos\theta_A (= |\sqrt{g_b g_c}|) \times \sqrt{\mathcal{B}(A^0 \to \mu^+\mu^-)}$, independent of $\tan\beta$, is very close to zero especially in the low-mass region [21]. However, this BESIII limit [21] is still an order of magnitude above the theoretical predictions [4]. BESIII has recently accumulated about 39 times more J/ψ events in comparison to the previous measurement [21], and these can be utilized to discover the A^0 or exclude parameter space of the NMSSM [22].

This paper describes the search for di-muon decays of a CP-odd light Higgs boson in radiative decays of J/ψ using 9 billion J/ψ events collected by the BESIII detector in 2009, 2018, and 2019 [22]. Because muon particle identification (PID) was not available for the J/ψ data collected in 2012, we exclude this data sample for the A^0 search.

II. BESIII DETECTOR AND MONTE CARLO SIMULATION

The BESIII detector [23] records symmetric e^+e^- collisions provided by the BEPCII storage ring [24], which operates with a peak luminosity of 1×10^{33} cm^{-2} s^{-1} in the center-of-mass energy range from 2.0 to 4.95 GeV. BESIII has collected large data samples in this energy region [25]. The cylindrical core of the BESIII detector covers 93% of the full solid angle and consists of a helium-based multilayer drift chamber (MDC), a plastic scintillator time-of-flight system (TOF), and a CsI(Tl) electromagnetic calorimeter (EMC), which are all enclosed in a superconducting solenoidal magnet providing a 1.0 T magnetic

field. The solenoid is supported by an octagonal flux-return yoke with resistive plate counter muon identification modules interleaved with steel. The MDC measures the momentum of charged particles with a resolution of 0.5% at 1 GeV/c. The EMC measures the photon energies with a resolution of 2.5% (5%) at 1 GeV in the barrel (endcap) region. The time resolution of the TOF in the barrel region is 68 ps. The time resolution of the TOF in the endcap region was 110 ps before 2015 and was improved to be 60 ps after upgrading with the multi-gap resistive plate chambers. Muons with momentum above 0.5 GeV/c are identified by the iron flux return of the magnet instrumented with about 1272 m^2 of resistive plate muon counters (MUC) arranged in nine (eight) layers in the barrel (endcaps).

Simulated Monte Carlo (MC) events based on GEANT4 [26] are used to optimize the event selection criteria, to study the potential backgrounds, and to determine the detector acceptance. A MC sample of 9.0 billion inclusive J/ψ events is used for the background studies with the generic TopoAna tool [27]. The known J/ψ decay modes are generated by the EVTGEN generator [28] with branching fractions taken from the Particle Data Group (PDG) [29], and the remaining unknown decay modes by LUNDCHARM [30]. The final state radiation corrections are included in the MC simulation using PHOTOS [31]. The production of the J/ψ resonance through e^+e^- annihilation including the beam-energy spread and the initial-state-radiation (ISR) is simulated by the KKMC [32]. A 2.93 fb^{-1} $\psi(3770)$ data sample [33,34] is used to study the background from the quantum electrodynamics (QED) process of $e^+e^- \to \gamma\mu^+\mu^-$. To compute the detection efficiency, we generate 0.12 million simulated signal MC events at 23 different Higgs mass points ranging from 0.212 to 3.0 GeV/c^2 with a phase-space model for the $A^0 \to \mu^+\mu^-$ decay and a P-wave model for the $J/\psi \to \gamma A^0$ decay [28].

III. DATA ANALYSIS

We select events with two oppositely charged tracks and at least one photon candidate. A photon candidate, reconstructed with clusters of energy deposited in the EMC, is selected with a minimum energy of 25 MeV in the barrel region ($|\cos\theta| < 0.8$) or 50 MeV in the end-cap region ($0.86 < |\cos\theta| < 0.92$). The energy deposited in the nearby TOF is included to improve the energy resolution and reconstruction efficiency. The angle between a photon and the nearest extrapolated track in the EMC is required to be larger than 10 degrees to remove bremsstrahlung photons. The EMC timing is required to be within 700 ns relative to the event start time to suppress electronic noise and energy deposits unrelated to the signal events.

Charged tracks are reconstructed from the ionization signals measured by the MDC and are required to be in the MDC detection acceptance region of $|\cos\theta| < 0.93$, where θ is the angle of the charged track with the z axis, which is the axis of the MDC. Further, their points of closest approach to the z-axis must be within ± 10 cm from the interaction point along the z direction and within ± 1 cm in the plane perpendicular to z. To suppress contamination by electrons and pions, both charged tracks are required to satisfy the following selection criteria: (1) $E^{\mu}_{\rm cal}/p < 0.9\ c$, (2) $0.1 < E^{\mu}_{\rm cal} < 0.3$ GeV, and (3) the absolute value of the time difference between the TOF and expected muon time ($\Delta t^{\rm TOF}$) must be less than 0.26 ns. Here, $E^{\mu}_{\rm cal}$ is the energy deposited in the EMC by the μ^+/μ^- particle, and p is the momentum of the charged muon track. To further improve the purity of muons, one of the charged tracks is required to have its penetration depth in the MUC be greater than $(-40.0 + 70 \times p/({\rm GeV}/c))$ cm for $0.5 \le p \le 1.1$ GeV/c and 40 cm for $p > 1.1$ GeV/c.

The two muon tracks are required to originate from a common vertex by performing a vertex fit to form an A^0 candidate. A four-constraint (4C) kinematic fit is performed with the two charged tracks and one of the photon candidates in order to improve the mass resolution of the A^0 candidate. If there is more than one $\gamma\mu^+\mu^-$ candidate, the candidate with the minimum value of the χ^2 from the 4C kinematic fit ($\chi^2_{\rm 4C}$) is selected, and the $\chi^2_{\rm 4C}$ is required to be less than 40 to reject backgrounds from $J/\psi \to \pi^+\pi^-\pi^0$ and $e^+e^- \to \gamma\pi^+\pi^-\pi^0$. We reject fake photons by requiring the dimuon invariant mass ($m_{\mu^+\mu^-}$) obtained from the 4C kinematic fit to be less than 3.04 GeV/c^2. To suppress backgrounds from $e^+e^- \to \gamma\mu^+\mu^-$ and $J/\psi \to \mu^+\mu^-(\gamma)$, the absolute value of the cosine of the muon helicity angle ($\cos\theta^{\rm hel}_{\mu}$), defined as the angle between the direction of one of the muons and the direction of the J/ψ in the A^0 rest frame, is required to be less than 0.92.

After the above selection criteria, we determine the signal yield as a function of m_{A^0} in the interval of $0.212 \le m_{A^0} \le 3.0$ GeV/c^2 by performing a series of one-dimensional unbinned extended maximum likelihood (ML) fits to the reduced mass, $m_{\rm red} = \sqrt{m^2_{\mu^+\mu^-} - 4m^2_{\mu}}$ distribution of surviving events. Figure 1 shows the $m_{\rm red}$ distribution of surviving events together with the background predictions from various simulated MC samples and 2.93 fb^{-1} of $\psi(3770)$ data [33,34]. We use $m_{\rm red}$ rather than $m_{\mu^+\mu^-}$ because it is easier to model the nonpeaking background across the entire m_{A^0} region, in particular, the kinematic threshold region $m_{\mu^+\mu^-} \approx 2m_{\mu}$ ($m_{\rm red} \approx 0$). The nonpeaking background is dominated by $e^+e^- \to \gamma\mu^+\mu^-$ and $J/\psi \to \mu^+\mu^-(\gamma)$, and the peaking background by $J/\psi \to \rho/\omega\pi$ and $J/\psi \to \gamma f$ ($f = f_2(1270), f_0(1500), f_0(1710)$) decays, where both ρ/ω and f decay to $\pi^+\pi^-$. The $m_{\rm red}$ distribution of data is generally well described by the background predictions, except in the low-mass region, where KKMC [32] fails to reproduce the ISR events for the $e^+e^- \to \gamma J/\psi, J/\psi \to \mu^+\mu^-$ process. This disagreement

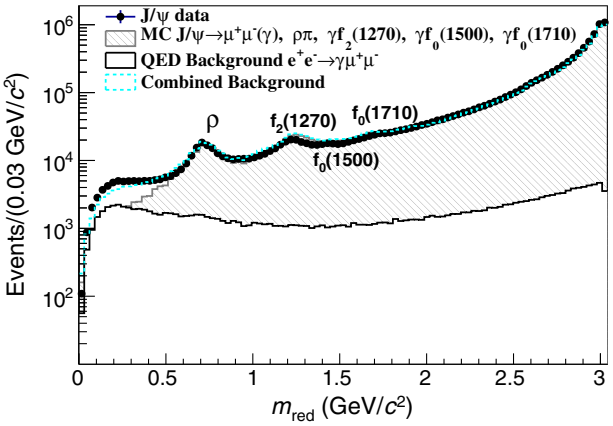

FIG. 1. The $m_{\rm red}$ distribution of data (black dot points with error bars), together with the background predictions of the QED $e^+e^- \to \gamma\mu^+\mu^-$ process from $\psi(3770)$ data (black histogram) and $J/\psi \to \rho\pi$, $\mu^+\mu^-(\gamma)$, γf $(f = f_2(1270), f_0(1500), f_0(1710))$ decays from MC samples of those processes (gray pattern histogram). The dashed cyan histogram represents the combined background.

has little impact on the search because the signal extraction procedure does not depend on the background predictions.

The fit function includes the contributions of signal, continuum background and peaking background components from ρ/ω, $f_2(1270)$, $f_0(1500)$, and $f_0(1710)$ mesons. Table I summarizes the $m_{\rm red}$ fit intervals for the various m_{A^0} points used to handle both nonpeaking and peaking backgrounds smoothly.

Simulated MC samples are used to develop the probability density functions (PDFs) of signal and backgrounds. The A^0 is assumed to be a scalar or pseudo-scalar particle with a very narrow decay width in comparison to the experimental resolution [35]. We describe the $m_{\rm red}$ distribution of the signal PDF by the sum of two Crystal Ball (CB) functions [36] with a common peak value and opposite side tails. The $m_{\rm red}$ resolution varies from 2 MeV/c^2 to 12 MeV/c^2 while the signal efficiency varies between 27% and 53% depending upon the muon momentum values at different A^0 mass points. We interpolate the signal efficiency and signal PDF parameters linearly between the mass points of the generated signal MC events. The nonpeaking background PDF is described by a function $\tanh(\sum_{l=1}^{5} p_l m_{\rm red}^l)$ in the threshold mass region of $0.212 \le m_{A^0} \le 0.40$ GeV/c^2, where p_l are the polynomial coefficients. This function provides a threshold like behavior in the low-mass region of the $m_{\rm red}$ distribution and passes through the origin when $m_{\rm red} = 0$. In the other mass regions, we use second, third, fourth, fifth or sixth-order Chebyshev polynomial function to describe the nonpeaking background PDFs detailed in Table I. We determine the initial parameters of these background PDFs using a cocktail MC sample of all possible nonpeaking backgrounds to achieve better agreement between data and the fit models.

TABLE I. The $m_{\rm red}$ fit intervals for various m_{A^0} points.

$m_{\rm red}$ fit interval (GeV/c^2)	m_{A^0} points (GeV/c^2)	Order of Polynomial function
0.002–0.45	0.212, 0.4	5th
0.3–0.65	0.401, 0.6	4th
0.4–1.06	0.601, 1.0	3rd
0.95–1.95	1.001, 1.8	2nd
1.7–2.5	1.802, 2.4	5th
2.3–2.7	2.402, 2.6	4th
2.5–2.9	2.602, 2.848	5th
2.75–3.0	2.85, 2.90	6th
2.85–3.032	2.902, 3.0	5th

To take into account the well-known structure of the ρ-ω interference, we describe the peaking background PDF of the $m_{\rm red}$ distribution with the Gounaris and Sakurai (GS) function in the range of $0.4 \le m_{\rm red} \le 1.06$ GeV/c^2 [37]. The fit formula, detailed in Ref. [38], is the same as that used previously by the *BABAR* [38] and BESIII [34] experiments in the measurement of the $e^+e^- \to \pi^+\pi^-$ cross section in the ρ/ω mass region. The amplitudes for the higher ρ states, $\rho(1450)$, $\rho(1700)$, and $\rho(2150)$, as well as the masses and widths of those states are taken from Ref. [38]. We fix the ω width according to the PDG [29] value and float the other parameters during the fit. We describe the peaking background PDFs corresponding to $f_2(1270)$, $f_0(1500)$ and $f_0(1710)$ resonances by the sum of the two CB functions [36] using the parameters determined from MC samples of $J/\psi \to \gamma f$, $f \to \pi^+\pi^-$ decays, where $f = f_2(1270)$, $f_0(1500)$, and $f_0(1710)$ mesons.

The search for the A^0 narrow resonance is performed in steps of approximately half the $m_{\rm red}$ resolution, i.e., 1 MeV/c^2 in the mass range of $0.22 \le m_{A^0} \le 1.5$ GeV/c^2 and 2.0 MeV/c^2 in the other m_{A^0} regions, with a total of 2 035 m_{A^0} points. The PDF parameters of the signal and peaking backgrounds of $J/\psi \to \gamma f$ are fixed while the nonpeaking background PDF, and the numbers of the signal, peaking, and nonpeaking background events are floated. Plots of the fit to the $m_{\rm red}$ distribution for two selected mass points are shown in Fig. 2.

The fit is repeated with alternative signal, peaking, and nonpeaking background PDFs to determine the systematic uncertainties for the numbers of signal events associated with the corresponding PDFs at each m_{A^0} point. The uncertainty associated with the signal PDF is studied by replacing the sum of the two CB functions with a "Cruijff" function [39]. The uncertainty associated with the ρ-ω peak is evaluated by varying the ρ and ω contributions in the formula of Eq. (26) of Ref. [38]. The uncertainty due to the peaking background of $J/\psi \to \gamma f$ is studied by replacing the sum of the two CB functions with the simulated MC samples of the corresponding decay processes convolved

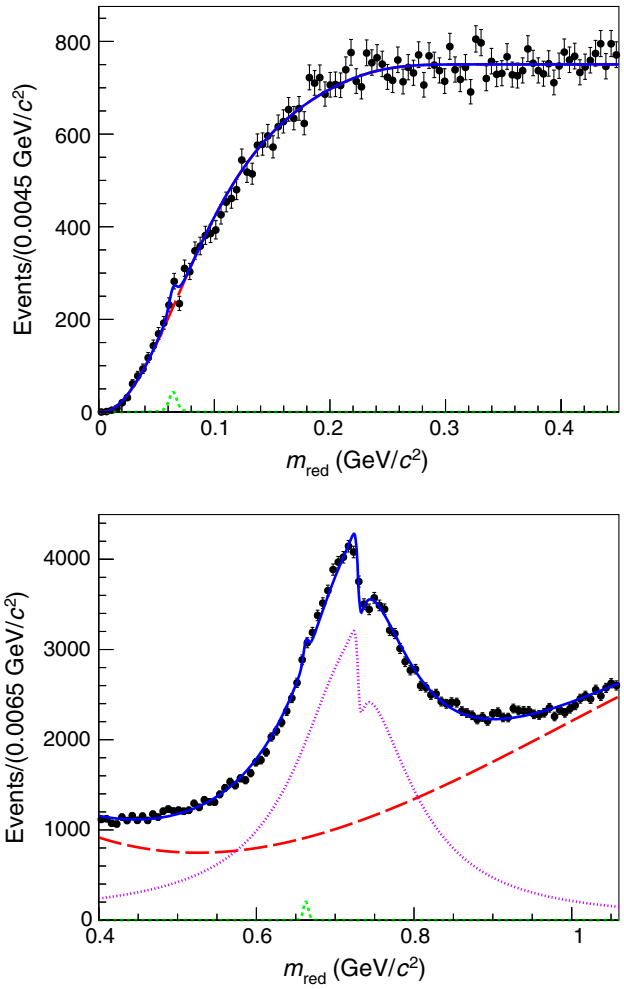

FIG. 2. Fits to the $m_{\rm red}$ distributions for (top) $m_{A^0} = 0.221$ GeV/c^2 and (bottom) $m_{A^0} = 0.696$ GeV/c^2. The corresponding local significance values at these mass points are observed to be 3.3σ and 3.5σ, respectively. Black dots with error bars represent the data, the red long-dashed curve the nonpeaking background, the pink dotted curve the peaking background, the green dashed curve the signal PDF, and the solid blue curve the total fit results. In the bottom figure, the well-known ρ-ω interference is taken care of by describing the peaking background PDF of the $m_{\rm red}$ distribution by a GS function [37,38], as described in the text.

with a Gaussian function whose parameters are floated during the fit. The uncertainty due to the nonpeaking background PDF is studied by replacing the $\tanh(\sum_{l=1}^{5} p_l m_{\rm red}^l)$ and nth order Chebyshev polynomial function with $\tanh(\sum_{l=1}^{6} p_l m_{\rm red}^l)$ and $(n+1)$th order Chebyshev polynomial functions, respectively, in the fit. The one with the largest signal yield among these fit scenarios is considered to produce the final result.

The product branching fraction of $J/\psi \to \gamma A^0$ and $A^0 \to \mu^+\mu^-$ as a function of m_{A^0} is calculated as

$$\mathcal{B}(J/\psi \to \gamma A^0) \times \mathcal{B}(A^0 \to \mu^+\mu^-) = \frac{N_{\rm sig}}{\epsilon \cdot N_{J/\psi}}, \quad (2)$$

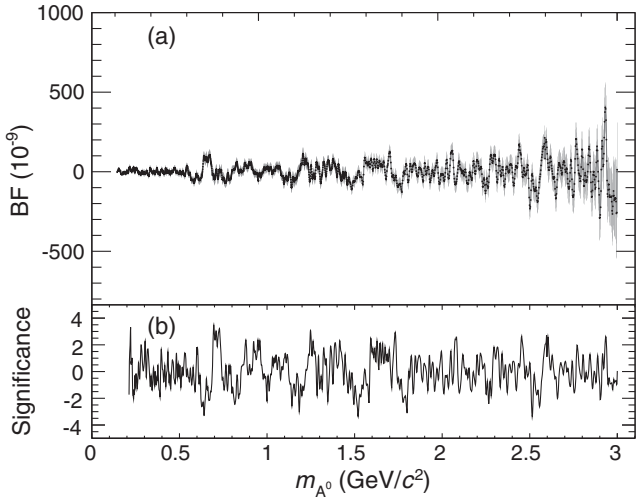

FIG. 3. (a) The product branching fractions $\mathcal{B}(J/\psi \to \gamma A^0) \times \mathcal{B}(A^0 \to \mu^+\mu^-)$ (BF) and (b) signal significance ($\mathcal{S}$) obtained from the fit as a function of m_{A^0}.

where $N_{\rm sig}$ is the number of signal events, ϵ is the signal selection efficiency, and $N_{J/\psi} = (8.998 \pm 0.039) \times 10^9$ is the number of J/ψ events. Figure 3 shows the plots of the product branching fractions $\mathcal{B}(J/\psi \to \gamma A^0) \times \mathcal{B}(A^0 \to \mu^+\mu^-)$ and the statistical significance, defined as $\mathcal{S} = \text{sign}(N_{\rm sig})\sqrt{2\ln(\mathcal{L}_{\rm max}/\mathcal{L}_0)}$, where $\mathcal{L}_{\rm max}(\mathcal{L}_0)$ is the maximum likelihood value for a fit with number of signal events being floated (fixed at zero). The largest upward local significance value is determined to be 3.5σ at $m_{A^0} = 0.696$ GeV/c^2. Based on a large ensemble of pseudoexperiments [18], the probability of observing a fluctuation of $\mathcal{S} \geq 3.5\sigma$ is estimated to be 12%. The corresponding global significance value is determined to be at the level of 1σ. Thus, we conclude that no evidence of Higgs production is found within the searched m_{A^0} regions.

IV. SYSTEMATIC UNCERTAINTIES

According to Eq. (2), the systematic uncertainties for the branching fraction measurement include those from the number of signal events, the reconstruction efficiency, and the number of J/ψ events. The uncertainties associated with the number of signal events originating from the PDF parameters of signal and backgrounds are considered by performing alternative fits at each m_{A^0} point.

Pseudo experiments are utilized to test the reliability of the fit procedures and compute the fit bias, which may appear due to imperfect signal and background modeling. The same fit procedure is performed in each pseudoexperiment. The resultant average difference between the input and output signal yields is determined to be 0.3 events. We consider it as an additive systematic uncertainty ($\sigma_{\rm add}$), which may affect the significance of any observation but does not scale with the reconstructed signal yield.

TABLE II. The fit bias and multiplicative sources of the systematic uncertainties. The systematic uncertainties associated with the signal, peaking, and nonpeaking background PDFs are taken as the largest difference of signal yield among the alternative fit scenarios at each m_{A^0} point as described in Sect. III.

Source	Uncertainty
Additive systematic uncertainties (events)	
Fit bias	0.3
Total	0.3
Multiplicative systematic uncertainties (%)	
Tracking	2.0
Photon detection efficiency	0.2
Depth in MUC	2.9–4.1
$E^{\mu}_{\rm cal}$	0.1
$\Delta t^{\rm TOF}$	Negl.
$\mathrm{Cos}\theta^{\rm hel}_{\mu}$	0.8
$\chi^2_{\rm 4C}$	1.8
J/ψ counting	0.7
Total	4.1–5.0

The uncertainties associated with the reconstruction efficiency and the number of J/ψ events do not affect the significance of any observation. Thus, we consider them as multiplicative systematic uncertainties ($\sigma_{\rm mult}$) and scale with the number of reconstructed signal events. The uncertainty associated with the reconstruction efficiency includes those from tracking, PID, and the photon detection efficiency.

The uncertainty due to MDC tracking is determined to be 1% per track using the high statistics control samples of $J/\psi \to \rho\pi$ and $J/\psi \to p\bar{p}\pi^+\pi^-$. A total of 2.0% systematic uncertainty is assigned for the two charged tracks in this analysis. The systematic uncertainty associated with the photon reconstruction efficiency is determined using a control sample of $e^+e^- \to \gamma\mu^+\mu^-$ in which the ISR photon is predicted using the four momenta of the two charged tracks. This sample also includes the dominant contribution from $J/\psi \to \gamma\pi^+\pi^-$ decay, including all the possible intermediate resonances. The relative difference in efficiency between data and MC is found to be 0.2%, which is considered as a systematic uncertainty.

A control sample of $J/\psi \to \mu^+\mu^-(\gamma)$ is used to evaluate the systematic uncertainty due to the muon PID, $\cos\theta^{\rm hel}_{\mu}$, and $\chi^2_{\rm 4C}$ requirements. In this sample, one track is tagged with a tight muon PID. The final uncertainty associated with the muon PID also takes into account the fraction of events with one or two tracks identified as muons obtained from the simulated signal MC sample. The corresponding uncertainties, computed as the relative change in efficiency between data and MC, are determined to be $(2.9-4.1)\%$, 0.8% and 1.8%, respectively. The systematic uncertainty due to the number of J/ψ events is 0.3% using J/ψ inclusive hadronic events. Table II summarizes the fit bias and multiplicative sources of the systematic uncertainties, where we obtain the total $\sigma_{\rm mult}$ by adding the individual ones in quadrature. The total $\sigma_{\rm mult}$ varies between 4.1% to 5.0% depending on the Higgs mass point. The final systematic uncertainty is calculated as $\sqrt{\sigma^2_{\rm add} + (\sigma_{\rm mult} \times N_{\rm sig})^2}$.

V. RESULT

Since no evidence of Higgs production is found, we set 90% confidence level (CL) upper limits on the product branching fractions $\mathcal{B}(J/\psi \to \gamma A^0) \times \mathcal{B}(A^0 \to \mu^+\mu^-)$ as a function of m_{A^0} using a Bayesian method [29] after incorporating the systematic uncertainty by smearing the likelihood curve with a Gaussian function having a width equal to the systematic uncertainty. The limits vary in the range of $(1.2-778.0)\times 10^{-9}$ for the Higgs mass region of $0.212 \le m_{A^0} \le 3.0$ GeV/c^2 depending on the m_{A^0} point, as shown in Fig. 4. The new measurement has a 6–7 times improvement over the previous BESIII measurement [21].

To compare our results with the *BABAR* measurement [18], we also compute 90% CL upper limits on the effective Yukawa coupling of the Higgs fields to the bottom-quark pair $g_b(=g_c\tan^2\beta)\times\sqrt{\mathcal{B}(A^0\to\mu^+\mu^-)}$ as a function of m_{A^0} for different values of $\tan\beta$ using Eq. (1) as shown in Fig. 5. Our new measurement is slightly better than the *BABAR* measurement [18] in the low-mass region for $\tan\beta = 1.0$.

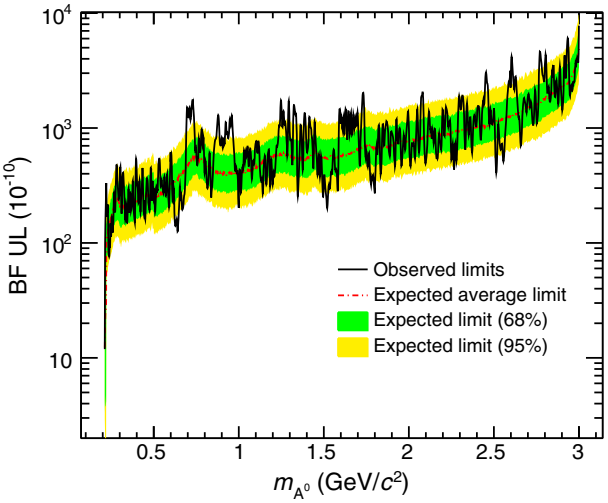

FIG. 4. The 90% CL upper limits on the product branching fractions $\mathcal{B}(J/\psi \to \gamma A^0) \times \mathcal{B}(A^0 \to \mu^+\mu^-)$ versus m_{A^0} including all the uncertainties, together with the expected limits computed using a large number of pseudoexperiments. The inner and outer bands correspond to 68% and 95% of the expected limit values and include the statistical uncertainties only.

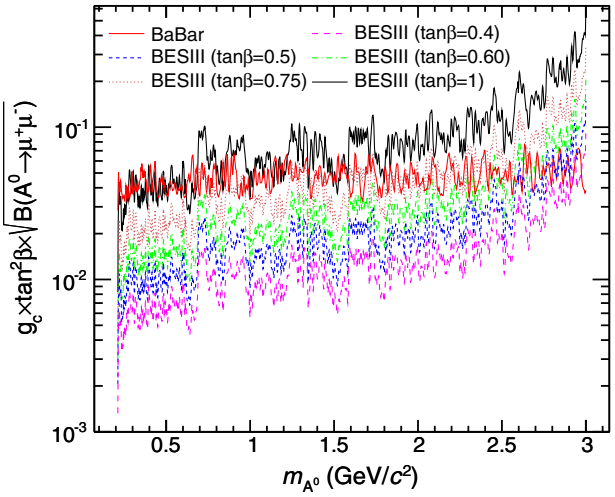

FIG. 5. The 90% CL upper limits on the effective Yukawa coupling of the Higgs field to the bottom-quark pair $g_b(= g_c \tan^2\beta) \times \sqrt{\mathcal{B}(A^0 \to \mu^+\mu^-)}$ as a function of m_{A^0} for different values of $\tan\beta$ together with the *BABAR* measurement. Our results are slightly better than the *BABAR* measurement in the low mass region for $\tan\beta = 1$.

VI. SUMMARY

We search for di-muon decays of A^0 in $J/\psi \to \gamma A^0$ using 9.0 billion J/ψ events collected by the BESIII detector. No evidence of Higgs production is found, and we set 90% CL upper limits on product branching fractions $\mathcal{B}(J/\psi \to \gamma A^0) \times \mathcal{B}(A^0 \to \mu^+\mu^-)$ in the range of $(1.2 - 778.0) \times 10^{-9}$ for $0.212 \le m_{A^0} \le 3.0$ GeV/c^2. This result has an improvement by a factor of 6-7 over the previous BESIII measurement [21], and is better than the *BABAR* measurement [18] for $m_{A^0} \le 0.7$ GeV/c^2 for $\tan\beta = 1$. Thus, our measurement is more stringent for $m_{A^0} \le 0.7$ GeV/c^2 over the existing experimental results [18–21,40]. The new BESIII limit is also lower than the theoretical prediction at the threshold Higgs mass point of 0.212 GeV/c^2, and thus constrains a large fraction of the parameter space of the new physics models, including NMSSM [3,4,17].

ACKNOWLEDGMENTS

The BESIII collaboration thanks the staff of BEPCII, the IHEP computing center and the supercomputing center of USTC for their strong support. This work is supported in part by National Key R&D Program of China under Contracts No. 2020YFA0406300, No. 2020YFA0406400; National Natural Science Foundation of China (NSFC) under Contracts No. 11335008, No. 11625523, No. 11625523, No. 11635010, No. 11735014, No. 11822506, No. 11835012, No. 11935015, No. 11935016, No. 11935018, No. 11961141012, No. 12022510, No. 12025502, No. 12035009, No. 12035013, No. 12035013, No. 12061131003, No. 11705192, No. 11950410506, No. 12061131003; the Chinese Academy of Sciences (CAS) Large-Scale Scientific Facility Program; Joint Large-Scale Scientific Facility Funds of the NSFC and CAS under Contracts No. U1732263, No. U1832207, No. U1832103, No. U2032111; CAS Key Research Program of Frontier Sciences under Contract No. QYZDJ-SSW-SLH040; 100 Talents Program of CAS; INPAC and Shanghai Key Laboratory for Particle Physics and Cosmology; ERC under Contract No. 758462; European Union Horizon 2020 research and innovation programme under Contract No. Marie Sklodowska-Curie grant agreement No. 894790; German Research Foundation DFG under Contracts Nos. 443159800, Collaborative Research Center CRC 1044, FOR 2359, FOR 2359, GRK 214; Istituto Nazionale di Fisica Nucleare, Italy; Ministry of Development of Turkey under Contract No. DPT2006K-120470; National Science and Technology fund; Olle Engkvist Foundation under Contract No. 200-0605; STFC (United Kingdom); The Knut and Alice Wallenberg Foundation (Sweden) under Contract No. 2016.0157; The Royal Society, UK under Contracts No. DH140054, No. DH160214; The Swedish Research Council; U.S. Department of Energy under Contracts No. DE-FG02-05ER41374, No. DE-SC-0012069.

[1] P. W. Higgs, Phys. Lett. **12**, 132 (1964); P. W. Higgs, Phys. Rev. Lett. **13**, 508 (1964); P. W. Higgs, Phys. Rev. **145**, 1156 (1966); F. Englert and R. Brout, Phys. Rev. Lett. **13**, 321 (1964); G. S. Guralnik, C. R. Hagen, and T. W. B. Kibble, Phys. Rev. Lett. **13**, 585 (1964).

[2] G. Aad *et al.* (Atlas Collaboration), Phys. Lett. B **716**, 129 (2012); S. Chatrchyan *et al.* (CMS Collaboration), Phys. Lett. B **716**, 3061 (2012).

[3] G. Hiller, Phys. Rev. D **70**, 034018 (2004); R. Dermisek and J. F. Gunion, Phys. Rev. Lett. **95**, 041801 (2005).

[4] R. Dermisek, J. F. Gunion, and B. McElrath, Phys. Rev. D **76**, 051105 (2007).

[5] J. Steggermann, Annu. Rev. Nucl. Part. Sci. **70**, 197 (2020).

[6] H. E. Haber and G. L. Kane, Phys. Rep. **117**, 75 (1985).

[7] A. Delgado, C. Kolda, and A. D. Puente, Phys. Lett. B **710**, 460 (2012).

[8] F. Wilczek, Phys. Rev. Lett. **39**, 1304 (1977).
[9] M. L. Mangano and P. Nason, Mod. Phys. Lett. A **22**, 1373 (2007).
[10] P. Nason, Phys. Lett. B **175**, 223 (1986).
[11] R. Barbieri, R. Gatto, R. Kögerler, and Z. Kunszt, Phys. Lett. B **57**, 455 (1975).
[12] M. Beneke, A. Signer, and V. A. Smirnov, Phys. Rev. Lett. **80**, 2535 (1998).
[13] R. Dermisek and J. F. Gunion, Phys. Rev. D **81**, 075003 (2010); F. Domingo, J. High Energy Phys. 04 (2011) 016.
[14] P. Fayet, Phys. Rev. D **75**, 115017 (2007); Phys. Lett. B **675**, 267 (2009).
[15] P. Fayet, Nucl. Phys. **B187**, 184 (1981); H. B. Li and T. Luo, Phys. Lett. B **686**, 249 (2010).
[16] M. Lisanti and J. G. Wacker, Phys. Rev. D **79**, 115006 (2009).
[17] P. Fayet and M. Mezard, Phys. Lett. B **104**, 226 (1981); P. Fayet, Phys. Rev. D **103**, 035034 (2021).
[18] J. P. Lees *et al.* (*BABAR* Collaboration), Phys. Rev. D **87**, 059903(R) (2013); V. Prasad, Ph.D. thesis, Report No. SLAC-R-1008, 2013 (unpublished).
[19] W. Love *et al.* (CLEO Collaboration), Phys. Rev. Lett. **101**, 151802 (2008).
[20] S. Chatrchyan *et al.* (CMS Collaboration), Phys. Rev. Lett. **109**, 121801 (2012).
[21] M. Ablikim *et al.* (BESIII Collaboration), Phys. Rev. D **93**, 052005 (2016).
[22] http://bes3.ihep.ac.cn/doc/3313.html.
[23] M. Ablikim *et al.* (BESIII Collaboration), Nucl. Instrum. Methods Phys. Res., Sect. A **614**, 345 (2010).
[24] C. H. Yu *et al.*, *Proceedings of IPAC2016, Busan, Korea, 2016*, 10.18429/JACoW-IPAC2016-TUYA01.
[25] M. Ablikim *et al.* (BESIII Collaboration), Chin. Phys. C **44**, 040001 (2020).
[26] S. Agostinelli *et al.* (GEANT Collaboration), Nucl. Instrum. Methods Phys. Res., Sect. A **506**, 250 (2003).
[27] X. Y. Zhou, S. X. Du, G. Li, and C. P. Shen, Comput. Phys. Commun. **258**, 107540 (2021).
[28] D. J. Lange, Nucl. Instrum. Methods Phys. Res., Sect. A **462**, 152 (2001); R. G. Ping, Chin. Phys. C **32**, 243 (2008).
[29] P. A. Zyla *et al.* (Particle Data Group), Prog. Theor. Exp. Phys. **2020**, 083C01 (2020).
[30] J. C. Chen, G. S. Huang, X. R. Qi, D. H. Zhang, and Y. S. Zhu, Phys. Rev. D **62**, 034003 (2000).
[31] E. Barberio and Z. Was, Comput. Phys. Commun. **79**, 291 (1994).
[32] S. Jadach, B. F. L. Ward, and Z. Was, Phys. Rev. D **63**, 113009 (2001).
[33] M. Ablikim *et al.* (BESIII Collaboration), Chin. Phys. C **37**, 123001 (2013).
[34] M. Ablikim *et al.* (BESIII Collaboration), Phys. Lett. B **753**, 629 (2016).
[35] E. Fullana and M. A. Sanchis-Lozano, Phys. Lett. B **653**, 67 (2007).
[36] J. E. Gaiser, Ph.D. thesis, Report No. SLAC-R-255, 1982 (unpublished); M. J. Oreglia, Ph.D. thesis, Report No. SLAC-R-236, 1980 (unpublished); T. Skwarnicki, Ph.D. thesis, Report No. DESY-F-31-86-02, 1986 (unpublished).
[37] G. J. Gounaris and J. J. Sakurai, Phys. Rev. Lett. **21**, 244 (1968).
[38] J. P. Lees *et al.* (*BABAR* Collaboration), Phys. Rev. D **86**, 032013 (2012).
[39] The Cruijff function is an asymmetric Gaussian function having a common mean (μ), different left-right resolutions ($\sigma_{L,R}$) and non-Gaussian tails ($\alpha_{L,R}$): $f(x) = \exp((x-\mu)^2/(2\sigma_{L,R}^2 + \alpha_{L,R}(x-\mu)^2))$.
[40] M. Ablikim *et al.* (BESIII Collaboration), Phys. Rev. D **85**, 092012 (2012).